International Journal of Smart Grid and Clean Energy

Analysis of electric field intensity and temperature distribution with various permittivity in supercapacitor by 3-D FEM

Padej Pao-la-or, Phonrut Bousungnoenb

School of Electrical Engineering, Institute of Engineering, Suranaree University of Technology, Nakhon Ratchasima 30000, Thailand

Abstract

This paper presents a simulation of electric potential distribution, electric field intensity and temperature in the spiral wound supercapacitor. The paper simulation using the 3-D finite element method that all coded by MATLAB program and show the graphical representation for electric potential, the electric field intensity and temperature of inner part for a supercapacitor and studies the permittivity of the electrolyte that affect the electric field intensity and temperature of supercapacitor. The simulation results show an electric field intensity and temperature of the inner part with various electrolytes including KOH and sodium iodide in various solvents electrolyte. Solvents of sodium iodide consist of CH_3OH, $(CH_3)_2SO$, $HCONH_3$ and $HCONHCH_3$ that have different relative permittivity. It can indicate to the working process of supercapacitor.

Keywords: Supercapacitor, electric field intensity, temperature, 3-D finite element method, permittivity

1. Introduction

At present, supercapacitors are popular as a source of electrical energy or used in backup power applications because of their long lifespan. Supercapacitors are electronic devices that have an unusually high energy density when compared to common capacitors [1]. However, supercapacitors have many advantages such as high efficiency, fast dynamic response, high capacitance, high level of stability and wide temperature operating range [2-4]. Supercapacitors exploit the electrostatic separation between electrolyte and high surface area electrodes, typically activated carbon [5][6]. Due to the low rated voltage cell of a supercapacitor, the series and parallel connection of supercapacitors are used to increase the energy storage capacity or high voltage requirement [7].

The finite element method (FEM) is a numerical technique used to perform finite element analysis (FEA) of any given physical phenomenon. The analytical solution of problems generally requires the solution to boundary value problems for partial differential equations (PDE) it can utilize to solve problems in electric field intensity [8] and heat transfer [9] of supercapacitor.

This paper will discuss on electric field intensity inside supercapacitor in activated carbon electrode layer and temperature distribution by using the 3-D finite element method. The finite element modeling of a supercapacitor in section 2, electrostatics analysis of supercapacitor in section 3 and thermal analysis of supercapacitor in section 4. Section 5 presents the 3-D FEM simulation result, and section 6 presents the conclusion of the study.

* Manuscript received August 12, 2019; revised June 4, 2020.
Corresponding author. *E-mail address*: padej@sut.ac.th.
doi: 10.12720/sgce.9.4.768-777

2. The Finite Element Modeling of Supercapacitor

In this paper study is the inner part of the spiral wound stacked supercapacitor produced by the domestic manufacturer, which is made up of the aluminum shell, phenolic cover and the inner part, and the dimension is 21 mm × 44 mm (Diameter × Length, lead wire is excluded) [9]. The structure is shown in Fig. 1. The inner part is a stackable structure that consists of the aluminum current collector, polypropylene separator and activated carbon electrode with KOH organic electrolyte system [10] stacked in layers.

In this paper study inner part of supercapacitor by using SOLIDWORK program to mesh the entity model shown in Fig. 2. by using linear tetrahedron elements. The whole element model consists of 33,873 elements and 6,449 nodes.

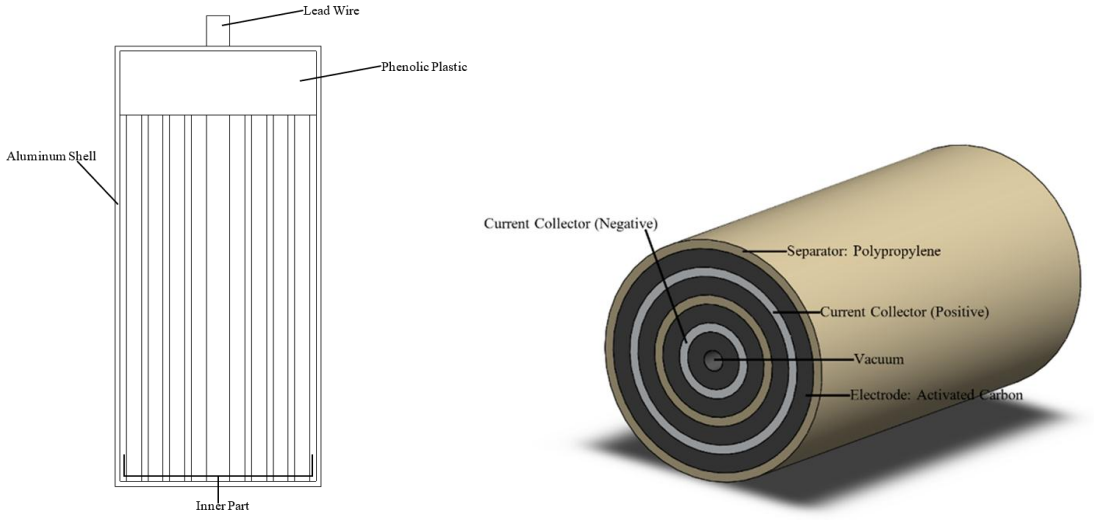

(a) (b)

Fig. 1. Structure schematic of supercapacitor: (a) Details of supercapacitor and (b) Details of inner part

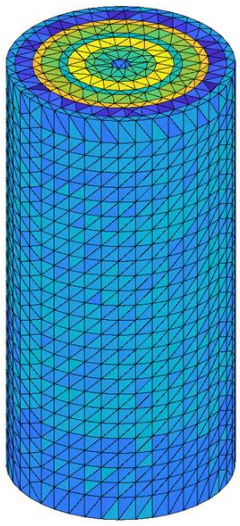

Fig. 2. Mesh of supercapacitor

3. Electrostatics Analysis of Supercapacitors

The partial differential equations (PDE) in Equation (1) is shown 3-D the Poisson's equation with the electrostatics is used to obtain the electric potential distribution in a supercapacitor.

$$\frac{\partial^2 U}{\partial x^2}+\frac{\partial^2 U}{\partial y^2}+\frac{\partial^2 U}{\partial z^2}=-\frac{\rho}{\varepsilon} \tag{1}$$

Where, U is electric potential (V), ρ is charge density (C/m^3) and ε is electric permittivity (F/m) derived from $\varepsilon=\varepsilon_o\varepsilon_r$ where, ε_o is the permittivity of free space is equal to 8.854×10^{-12} F/m and ε_r is relative permittivity

Formulating of the element interpolation function in three dimensions is derived from the Poisson's equations, assume the characteristics distribution of solution in the element by linear representation shown in Equation (2) [11].

$$U(x,y,z)=U_iN_i+U_jN_j+U_kN_k+U_lN_l \tag{2}$$

Where, N_i, N_j, N_k, N_l are the shape function in the element of node i, j, k, l respectively, and U_i, U_j, U_k, U_l are the electric potential at node i, j, k, l respectively. The shape function of each element is derived from Equation (3).

$$N_n=\frac{a_n+b_nx+c_ny+d_nz}{6V} \tag{3}$$

Where, n = i, j, k, l, and V is the volume of the element, which derived from Equation (4).

$$V=\frac{1}{6}\begin{vmatrix}1 & x_i & y_i & z_i\\ 1 & x_j & y_j & z_j\\ 1 & x_k & y_k & z_k\\ 1 & x_l & y_l & z_l\end{vmatrix} \tag{4}$$

The positional coefficient defined by

$$a_i=x_l\left(y_jz_k-y_kz_j\right)+x_k\left(y_lz_j-y_jz_l\right)+x_j\left(y_kz_l-y_lz_k\right) \qquad b_i=y_l\left(z_k-z_j\right)+y_k\left(z_j-z_l\right)+y_j\left(z_l-z_k\right)$$
$$a_j=x_l\left(y_kz_i-y_iz_k\right)+x_k\left(y_iz_l-y_lz_i\right)+x_i\left(y_lz_k-y_kz_l\right) \qquad b_j=y_l\left(z_i-z_k\right)+y_i\left(z_k-z_l\right)+y_k\left(z_l-z_i\right)$$
$$a_k=x_l\left(y_iz_j-y_jz_i\right)+x_j\left(y_lz_i-y_iz_l\right)+x_i\left(y_jz_l-y_lz_j\right) \qquad b_k=y_l\left(z_j-z_i\right)+y_j\left(z_i-z_l\right)+y_i\left(z_l-z_j\right)$$
$$a_l=x_k\left(y_jz_i-y_iz_j\right)+x_j\left(y_iz_k-y_kz_i\right)+x_i\left(y_kz_j-y_jz_k\right) \qquad b_l=y_k\left(z_i-z_j\right)+y_i\left(z_j-z_k\right)+y_j\left(z_k-z_i\right)$$

$$c_i=x_l\left(z_j-z_k\right)+x_j\left(z_k-z_l\right)+x_k\left(z_l-z_j\right) \qquad d_i=x_l\left(y_k-y_j\right)+x_k\left(y_j-y_l\right)+x_j\left(y_l-y_k\right)$$
$$c_j=x_l\left(z_k-z_i\right)+x_k\left(z_i-z_l\right)+x_i\left(z_l-z_k\right) \qquad d_j=x_l\left(y_i-y_k\right)+x_i\left(y_k-y_l\right)+x_k\left(y_l-y_i\right)$$
$$c_k=x_l\left(z_i-z_j\right)+x_i\left(z_j-z_l\right)+x_j\left(z_l-z_i\right) \qquad d_k=x_l\left(y_j-y_i\right)+x_j\left(y_i-y_l\right)+x_i\left(y_l-y_j\right)$$
$$c_l=x_k\left(z_j-z_i\right)+x_j\left(z_i-z_k\right)+x_i\left(z_k-z_j\right) \qquad d_l=x_k\left(y_i-y_j\right)+x_i\left(y_j-y_k\right)+x_j\left(y_k-y_i\right)$$

The formulating each element equations used the weighted residual method and the approximate results in Equation (1) which is equal residual function as follow Equation (5).

$$\varepsilon\left(\frac{\partial^2 U}{\partial x^2}+\frac{\partial^2 U}{\partial y^2}+\frac{\partial^2 U}{\partial z^2}\right)+\rho=R \tag{5}$$

Where, R is the residual function, and make the integration by parts using Gauss's theory as follow Equation (6).

$$\int_V\left(N_n\left[\varepsilon\left(\frac{\partial^2 U}{\partial x^2}+\frac{\partial^2 U}{\partial y^2}+\frac{\partial^2 U}{\partial z^2}\right)+\rho\right]\right)dv=0 \tag{6}$$

Equation (6) can be divided into two parts as follows

$$\int_V N_n\varepsilon\left(\frac{\partial^2 U}{\partial x^2}+\frac{\partial^2 U}{\partial y^2}+\frac{\partial^2 U}{\partial z^2}\right)dv+\int_V\left(N_n\rho\right)dv=0 \tag{7}$$

From equation (7) each element equation can be expressed in matrix form

$$[K]\{U\}=\{F\} \tag{8}$$

Where $[K]$ is the permittivity matrix of problem. From Equation (7) became the permittivity matrix depends on coordination x, y and z direction of each node as follow Equation (9).

$$[K]_{4x4}=\frac{\varepsilon}{36V}\begin{bmatrix} b_ib_i+c_ic_i+d_id_i & b_ib_j+c_ic_j+d_id_j & b_ib_k+c_ic_k+d_id_k & b_ib_l+c_ic_l+d_id_l \\ b_jb_i+c_jc_i+d_jd_i & b_jb_j+c_jc_j+d_jd_j & b_jb_k+c_jc_k+d_jd_k & b_jb_l+c_jc_l+d_jd_l \\ b_kb_i+c_kc_i+d_kd_i & b_kb_j+c_kc_j+d_kd_j & b_kb_k+c_kc_k+d_kd_k & b_kb_l+c_kc_l+d_kd_l \\ b_lb_i+c_lc_i+d_ld_i & b_lb_j+c_lc_j+d_ld_j & b_lb_k+c_lc_k+d_ld_k & b_lb_l+c_lc_l+d_ld_l \end{bmatrix} \tag{9}$$

And $\{F\}$ is the source vector of a problem as follow (10).

$$[F]_{4\times1}=\frac{\rho V}{4}\begin{bmatrix}1\\1\\1\\1\end{bmatrix} \tag{10}$$

The result of the problem is derived from solving a linear equation for calculation of electric potential. Therefore, the electric field intensity can be calculated as follows Equation (11).

$$\mathrm{E}=-\nabla U \tag{11}$$

Where, E is an electric field intensity of the supercapacitor.

4. Thermal Analysis of Supercapacitors

Studying thermal in supercapacitor use PDEs thermal heat transfer equation as follow Equation (12). That used to obtain temperature distribution in supercapacitor.

$$k\frac{\partial}{\partial x}\frac{\partial T}{\partial x}+k\frac{\partial}{\partial y}\frac{\partial T}{\partial y}+k\frac{\partial}{\partial z}\frac{\partial T}{\partial z}+Q=\rho c\frac{\partial T}{\partial t} \tag{12}$$

Where, T is temperature (˚K), k is thermal conductivity (W/ ˚K.m^2), c is specific heat capacity (J/kg. ˚K), ρ is density (kg/m^3) and Q is internal heat generation (W/m^3) can be calculated as follows Equation (13)

$$Q=\mathrm{JE} \tag{13}$$

Where, J is current density (A/m^2) and E is electric field intensity (V/m^2)

From Equation (12), solving finite element method same as electrostatic analysis. Each element equation can be expressed in matrix form

$$[C]\{\dot{T}\}+\left(\left[K_c\right]+\left[K_h\right]\right)\{T\}=\{Q\}+\{\mathrm{q}_h\} \tag{14}$$

Where, $[C]$ is heat capacity matrix, $[K_C]$ is heat diffusion matrix, $[K_h]$ is heat convection matrix, $\{Q\}$ is internal heat generation load vector and $\{q_h\}$ is heat convection load vector can be obtained from

$$[C]=\frac{\rho cV}{20}\begin{bmatrix}2&1&1&1\\1&2&1&1\\1&1&2&1\\1&1&1&2\end{bmatrix} \tag{15}$$

$$\left[K_c\right]=\frac{k}{36V}\begin{bmatrix}b_ib_i+c_ic_i+d_id_i & b_ib_j+c_ic_j+d_id_j & b_ib_k+c_ic_k+d_id_k & b_ib_l+c_ic_l+d_id_l\\ b_jb_i+c_jc_i+d_jd_i & b_jb_j+c_jc_j+d_jd_j & b_jb_k+c_jc_k+d_jd_k & b_jb_l+c_jc_l+d_jd_l\\ b_kb_i+c_kc_i+d_kd_i & b_kb_j+c_kc_j+d_kd_j & b_kb_k+c_kc_k+d_kd_k & b_kb_l+c_kc_l+d_kd_l\\ b_lb_i+c_lc_i+d_ld_i & b_lb_j+c_lc_j+d_ld_j & b_lb_k+c_lc_k+d_ld_k & b_lb_l+c_lc_l+d_ld_l\end{bmatrix} \tag{16}$$

$$[K_h]=\frac{hV}{20}\begin{bmatrix}2&1&1&1\\1&2&1&1\\1&1&2&1\\1&1&1&2\end{bmatrix} \tag{17}$$

$$\{Q\}=\frac{QV}{4}\begin{bmatrix}1\\1\\1\\1\end{bmatrix} \tag{18}$$

$$\{q_h\}=\frac{hT_\infty V}{4}\begin{bmatrix}1\\1\\1\\1\end{bmatrix} \tag{19}$$

Where, h is convective heat transfer (kJ/kg) and T_∞ is ambient temperature (˚K)

From Equation (14), $\left\{\dot{T}\right\}$ is the derivative of temperature. Therefore, using the backward difference method as follows Equation (20) [12].

$$\left\{\dot{T}\right\}^{t+\Delta t}=\frac{\left\{T\right\}^{t+\Delta t}-\left\{T\right\}^{t}}{\Delta t} \tag{20}$$

5. 3-D FEM Simulation Result

The 3-D finite element method simulation in this paper is coded by MATLAB programming for calculated the electric field intensity and temperature distribution within supercapacitor.

5.1. Electrostatic model

For the simulation results, this paper has considered the electric potential of the spiral wound supercapacitor with each type of electrolyte by assuming electrolyte are made sodium iodide in various solvents. The simulated initial voltage cell of the supercapacitor is 2.7 V (+1.35 V in the positive side and -1.35 V in the negative side). Table 1 shows parameter simulation [13-17].

Table 1. Relative permittivity of components in supercapacitor and sodium iodide in various solvents electrolyte

components	material	relative permittivity (ε_r)
Current collector	Aluminum	10.8
Electrode	Activated carbon	14.1
Separator	Polypropylene	2.3
Electrolyte	KOH	76
	CH_3OH	33.2
	$(CH_3)_2SO$	47.1
	$HCONH_3$	109.5
	$HCONHCH_3$	182.4

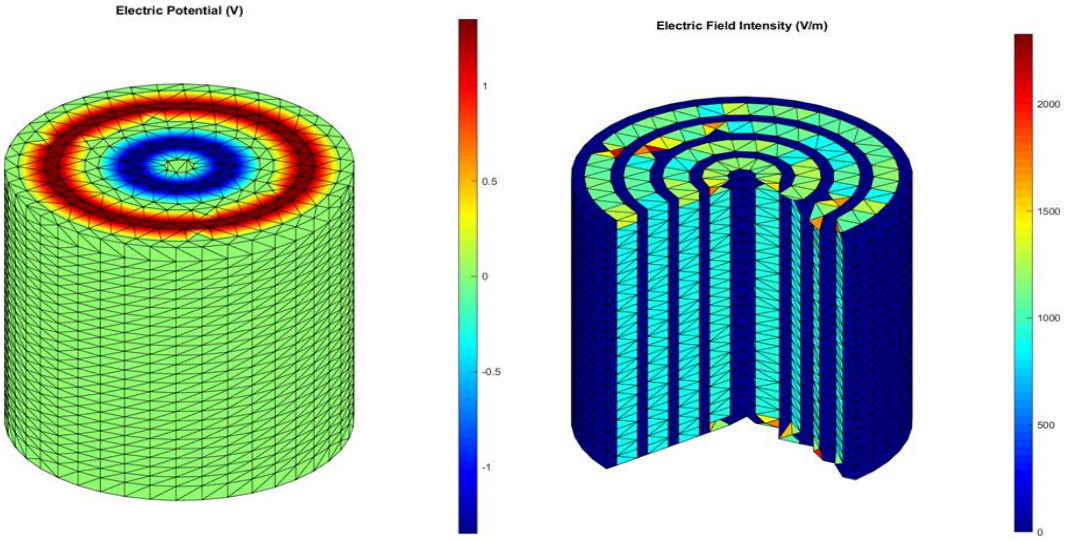

(a) (b)

Fig. 3. Electrostatic simulation result: (a) electric potential distribution and (b) electric field intensity

In Fig. 3 (a). the electric potential is fully distributed around the current collector (aluminum plate) as defined boundary conditions. In the positive voltage side, the electric potential will gradually decrease around the electrode (activated carbon) and reduced to zero at separator (polypropylene). In the negative voltage side, the electric potential will gradually increase around the electrode and increased to zero at the separator. In Fig. 3 (b). the electric field intensity distributed only in the area of electrodes (activated carbon), in current collector, separator and vacuum the electric field intensity are zero. Therefore, the simulation by using sodium iodide in various solvents electrolyte that different values of permittivity are cause electric field intensity decreases when permittivity is increased in exponential function as shown in Fig. 4.

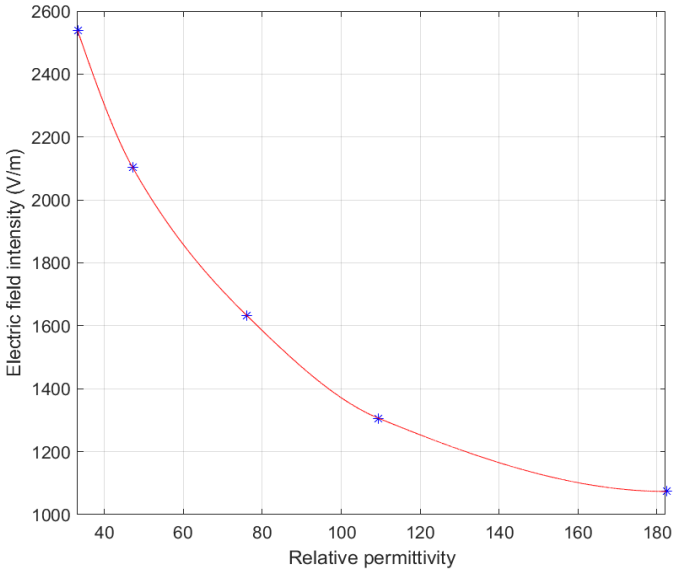

Fig. 4. Electric field intensity in the electrode layer with the value of the relative permittivity

5.2. Thermal model

The simulation parameter of thermal model shown in Table 2 [18] and the initial condition defines the ambient temperature is 28 ˚C. Assume the electrolyte solution does not gravitate on the inner part of the supercapacitor, do not have the convection and radiation in this region. On the external surface of the supercapacitor, heat transfer includes the heat convection to ambient temperature. Fig. 5. show the temperature distribution in supercapacitor with various electrolytes from the beginning to the constant.

Table 2. Parameter of thermal model

Materials	ρ (kg/m^3)	c (J/kg. ˚K)	k (W/ ˚K.m^2)
Aluminum	2700	900	238
Activated carbon	700	700	5
Polypropylene	1008.98	1978.16	0.3344

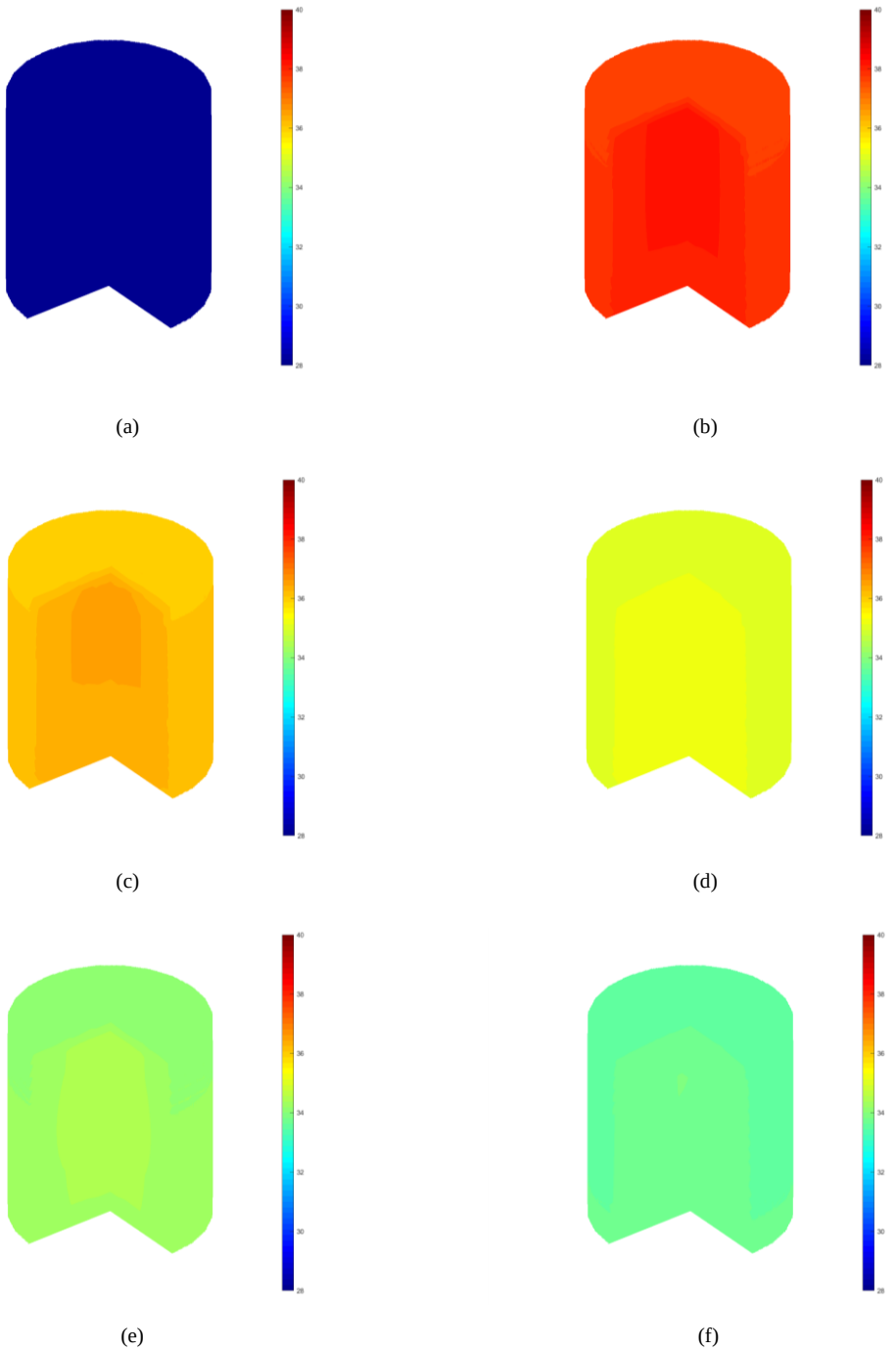

Fig. 5. Temperature distribution (˚C) in supercapacitor: (a) beginning (b) CH_3OH solvent electrolyte (c) $(CH_3)_2SO$ solvent electrolyte (d) KOH electrolyte (e) $HCONH_3$ solvent electrolyte and (f) $HCONHCH_3$ solvent electrolyte

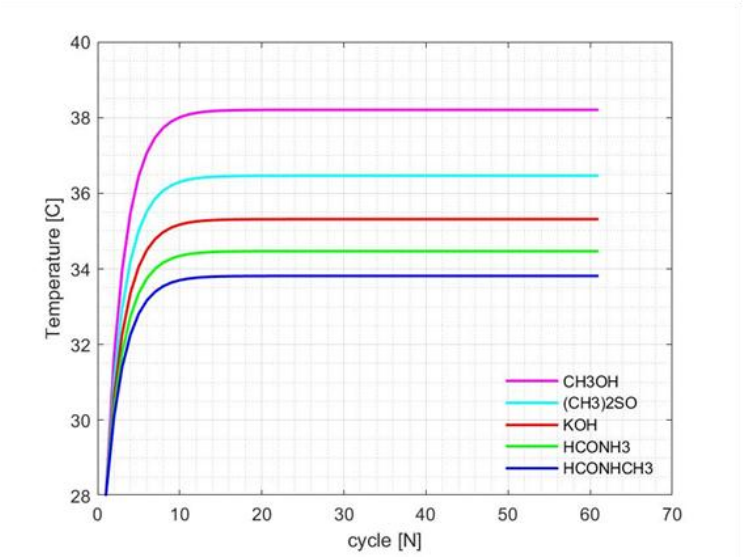

Fig. 6. Maximum temperature (˚C) of supercapacitor with various electrolyte per cycle

The simulation, the temperature of the supercapacitor will increase and stabilize at a certain value, which varies according to the type of electrolyte with a higher temperature in the middle then spread to the surrounding area. From Fig. 6. maximum temperature distribution in supercapacitor shown in Table 3.

Table 3. Maximum temperature of supercapacitor with various electrolytes

	CH_3OH	$(CH_3)_2SO$	KOH	$HCONH_3$	$HCONHCH_3$
Maximum temperature (˚C)	38.205	36.426	35.313	34.468	33.813

6. Conclusion

This paper simulation used the 3-D finite element method for solving the partial differential equation of electrostatic and thermal to illustrate the relationship between electrolytes and electric field intensity, which may affect the operation of the supercapacitor. Also, the simulation presents a value of the electric field intensity and temperature distribution in the electrode layer. The simulation results show that the electric field intensities decrease as the permittivity of electrolyte increases be the cause of temperature in supercapacitor decreases. For electrolytes consists of KOH and sodium iodide in various solvents, $HCONHCH_3$ makes the operating temperature of the supercapacitor is lowest. The efficacy of supercapacitor is based on the materials used to make electrodes, electrolyte and the internal structure design of the supercapacitor. Therefore, designing technology of the supercapacitor is the alternative way to increase the efficacy of the supercapacitor that leads to more performance.

Conflict of Interest

The authors declare no conflict of interest.

Author Contributions

Pao-la-or conducted the research; Bousungnoen analyzed the data; Pao-la-or and Bousungnoen wrote the paper; all authors had approved the final version.

Acknowledgements

This work was supported by School of Electrical Engineering, Institute of Engineering, Suranaree University of Technology.

References

[1] Simon P and Gogotsi Y. Materials for electrochemical capacitors, *Nature Materials*. Dec. 2008; 7(11): 845-854.
[2] Chan CC and Chau KT. *Modern Electric Vehicle Technology*. Oxford University Press, vol. 2001.
[3] Yao YY, Zhang DL and Xu DG. A study of supercapacitor parameters and characteristics. in *Proc. Power System Technology Conf.*, 2006; 1-4.
[4] Jiang L and Arnet BJ. Charging supercapacitors from low voltage with an induction machine. in *Proc. 2007 IEEE Vehicle Power and Propulsion Conf.*, 2007; 537-543.
[5] Tashima D, Taniguchi M, Ostubo M, Okazaki A and Araki S. Thickness dependence of carbon electrode on space charge of electric double layer capacitor. *Electrical Insulation and Dielectric Phenomena*, Vancouver, BC, Oct 14-17, 2007.
[6] Schneuwly A and Gallay R. Properties and applications of supercapacitors from the state-of-the-art to future trends. in *Proc. PCIM Conf.*, 2000: 1-10.
[7] K. Maneesut and U. Supatti, "Reviews of supercapacitor cell voltage equalizer topologies for EVs," 14th International Conference on Electrical Engineering/Electronics Computer Telecommunications and Information Technology (ECTI-CON 2017), pp. 608-611, Phuket Thailand, 2017.
[8] Jin-yan S, Li Z, and Ji-yan Z. The study of electric field of high-power supercapacitors. 14th Symposium on Electromagnetic Launch Technology (ELT 2008), 2008; 1-5, Victoria, BC, Canada.
[9] Kai W, Liwei L, Huaixian Y, Tiezhu Z. and Wubo W. (October 2015). Thermal Modelling Analysis of Spiral Wound Supercapacitor under Constant-Current Cycling. PLOS ONE. [Online]. Available: https://doi.org/10.1371/journal.pone.0138672
[10] Simon P. and Burke A. Nanostructured carbons: double-layer capacitance and more. *The Electrochemical Socity Interface*, 2008; 38-43.
[11] Vacharakup S, Peerasaksophol M, Kulworawanichpong T, and Pao-la-or P. Study of natural frequencies and characteristics of piezoelectric transformers by using 3-D finite element method. *Applied Mechanics and Materials*, 2012; 110-116: 61-66.
[12] Pao-La-Or P, and Amornsawatwattanaa I. Analysis of water temperature distribution in various type of absorber in solar thermal by 3-D finite element method. *International Journal of Smart Grid and Clean Energy*, July 2019; 8(4); 461-469.
[13] Jackson JD, *Classical Electrodynamics*, 3rd ed. New York: Wiley, 1998; 154.
[14] Singh R, and Ulrich RK. High and Low Dielectric Constant Materials. *The Electrochemical Socity Interface*, 1999; 26-30.
[15] Ramana CHVV, Ashok Kumar M, Kiran KABV, and Venumadhav K. Dielectric Constant measurement for solids using discrete components. *International Journal of Advanced Engineering and Global Technology (IJAEGT)*. 2013; 1(4): 163-167.
[16] Zaini MAA, Aini NMN, Kamaruddin MJ, Yeow YK and Setapar SHM. Dielectric properties of potassium hydroxide-treated palm kernel shell. *Jurnal of Teknologi*, 2015; 74(7): 13-18.
[17] Winsor P and Cole RH. (1982). Dielectric properties of electrolyte solutions. 1. Sodium iodide in seven solvents at various temperatures. *The Journal of Physical Chemistry*. [Online]. 86(13). pp. 2486-2490. Available: https://pubs.acs.org/doi/pdf/10.1021/j100210a049
[18] Li Y, Wang S, Zheng M, & Liu J. Thermal behavior analysis of stacked-type supercapacitors with different cell structures. *CSEE Journal of Power and Energy Systems*, 2018; 4(1): 112-120.